Transport of Viruses Through Saturated and Unsaturated Columns Packed with Sand

ARTICLE *in* TRANSPORT IN POROUS MEDIA · MAY 2008

Impact Factor: 1.55 · DOI: 10.1007/s11242-008-9239-3

2 AUTHORS:

Robert Anders
United States Geological Sur…
16 PUBLICATIONS **178** CITATIONS

SEE PROFILE

Constantinos V. Chrysikopo…
Technical University of Crete
143 PUBLICATIONS **2,004** CITATIONS

SEE PROFILE

Transp Porous Med (2012) 94:617–642
DOI 10.1007/s11242-012-0015-z

Transport of *Pseudomonas putida* in a 3-D Bench Scale Experimental Aquifer

Constantinos V. Chrysikopoulos · Vasiliki I. Syngouna · Ioanna A. Vasiliadou · Vasileios E. Katzourakis

Received: 15 November 2011 / Accepted: 19 April 2012 / Published online: 22 May 2012

Abstract This study is focused on the transport of *Pseudomonas (P.) putida* bacterial cells in a 3-D model aquifer. The pilot-scale aquifer consisted of a rectangular glass tank with internal dimensions: 120 cm length, 48 cm width, and 50 cm height, carefully packed with well-characterized quartz sand. The *P. putida* decay was adequately represented by a first-order model. Transport experiments with a conservative tracer and *P. putida* were conducted to characterize the aquifer and to investigate the bacterial behavior during transport in water saturated porous media. A 3-D, finite-difference numerical model for bacterial transport in saturated, homogeneous porous media was developed and was used to successfully fit the experimental data. Furthermore, theoretical interaction energy calculations suggested that the extended-DLVO theory seems to predict bacteria attachment onto the aquifer sand better than the classical DLVO theory.

Keywords Bacteria · Bench scale aquifer · Mathematical modeling · Attachment · Colloid stability · Extended DLVO

List of symbols

A_{123}	Hamaker constant (J) $(\mathrm{M\,L^2})/\mathrm{t^2}$
C	Dissolved or suspended aqueous phase concentration (M species)/$\mathrm{L^3}$
C^*	Concentration attached onto the solid phase (M species)/(M solids)
C_{eq}	Dissolved or suspended aqueous phase concentration at equilibrium (M species)/$\mathrm{L^3}$
C^*_{eq}	Concentration attached onto the solid phase at equilibrium (M species)/(M solids)
d_{c}	Sand grain diameter (L)
d_{p}	Particle diameter (L)
$\mathcal{D}_{\mathrm{AB}}$	Molecular diffusion coefficient ($\mathrm{L^2/t}$)
$\mathcal{D}_{\mathrm{e}}$	Effective diffusion coefficient ($\mathrm{L^2/t}$)

C. V. Chrysikopoulos (✉) · V. I. Syngouna · I. A. Vasiliadou · V. E. Katzourakis
Environmental Engineering Laboratory, Department of Civil Engineering, University of Patras, 26500 Patras, Greece
e-mail: gios@upatras.gr

D_x	Longitudinal hydrodynamic dispersion coefficient of species (L^2/t)
D_y	Lateral hydrodynamic dispersion coefficient of species (L^2/t)
D_z	Vertical hydrodynamic dispersion coefficient of species (L^2/t)
e	Charge of an electron (C)
F	General form of the source configuration ($M/(L^3\ t)$)
h	Separation distance between two approaching surfaces (L)
h_o	Minimum separation distance between two approaching surfaces (L)
I_s	Ionic strength (mol/L^3)
k_B	Boltzmann's constant, $(M\ L^2)/(t^2\ T)$ or (J/T)
k_c	Attachment (deposition) rate coefficient of species onto quartz sand (t^{-1})
k_r	Detachment rate coefficient of species from quartz sand (t^{-1})
K_d	Distribution coefficient L^3/(M solids)
K_{123}	Hydrophobic force constant (J) ($M\ L^2/t^2$)
L_x	Aquifer length in the x-direction (L)
L_y	Aquifer length in the y-direction (L)
L_z	Aquifer length in the z-direction (L)
m_n	nth Absolute temporal moment, defined in (14) (t^n)
M_n	nth Normalized temporal moment, defined in (15) (t^n)
mw_B	Molecular weight of solute B (M/mol)
n	Subscript indicating the order of the moment (−)
n_x	Number of discretization unit cells in the x-direction (−)
n_y	Number of discretization unit cells in the y-direction (−)
n_z	Number of discretization unit cells in the z-direction (−)
N_A	Avogadro's number (mol^{-1})
N_{Cr}	Courant number (−)
Pe	Peclet number (−)
r_b	Radius of the bacterial cell (L)
t	Time (t)
T	Temperature (K) T
U	Interstitial velocity (L/t)
V_A	Molar volume equal to mw_A/ρ_A (L^3/mol)
x	Longitudinal spatial coordinate (L)
y	Lateral spatial coordinate (L)
z	Vertical spatial coordinate (L)
z	Distance between the charged particle surface and its slipping plane (L)

Greek letters

α	Bruggeman exponent (−)
α_L	Longitudinal dispersivity (L)
α_{Ty}	Lateral dispersivity (L)
α_{Tz}	Vertical dispersivity (L)
β_i	Contact angle of material i (°)
ε	Dielectric constant of the suspending liquid ($C^2/(J\ L)$)
ε_0	Permittivity of free space ($C^2/(J\ L)$)
ε_r	Relative dielectric constant of the suspending liquid
ζ	Measured zeta potential of species and quartz grains (V)

θ	Porosity of the column material ((L^3 voids)/(L^3 solid matrix))
κ	Inverse Debye-Hückel length (L^{-1})
μ	Dynamic viscosity (M/(L t))
λ	Decay rate of species suspended in the liquid phase (t^{-1})
λ^*	Decay rate of species sorbed or attached onto the solid matrix (t^{-1})
λ_{AB}	Decay (Debye) length of water (L)
λ_w	Characteristic wavelength of the sphere–plate interactions (L)
ρ_A	Density of A (M/L^3)
ρ_b	Bulk density of the solid matrix (M/L^3)
σ_{Born}	Born collision parameter (L)
τ^*	Tortuosity (−)
Φ_{AB}	Lewis acid-base potential energy (J) ($M\,L^2/t^2$)
$\Phi_{AB(h_o)}$	Lewis acid-base free energy of interaction at $h = h_o$ (J/m^2)(M/t^2)
Φ_{max1}	Primary maximum of Φ_{tot} (J) ($M\,L^2/t^2$)
Φ_{min1}	Primary minimum of Φ_{tot} (J) ($M\,L^2/t^2$)
Φ_{min2}	Secondary minimum of Φ_{tot} (J) ($M\,L^2/t^2$)
Φ_{tot}	Total intersurface potential energy (J) ($M\,L^2$)/t^2
Φ_{vdW}	Van der Waals potential energy (J) ($M\,L^2$)/t^2
Φ_{dl}	Double layer potential energy (J) ($M\,L^2$)/t^2
Φ_{Born}	Born potential energy (J) ($M\,L^2$)/t^2
ψ	Surface potential (volts) ($M\,L^2$)/(t^3A)
ψ_B	Wilke–Chang parameter for solvent B (−)
ω	Number of time steps (−)

Abbreviations

AU	Absorbance units
CFU	Colony-forming units
DLVO	Derjaguin–Landau–Verwey–Overbeek
OD	Optical density
sdH_2O	Sterile distilled water
SL	Sampling location
sp	Sphere-plate
ss	Sphere–sphere
XDLVO	Extended DLVO

1 Introduction

The widespread contamination of groundwater with pathogens has resulted in an increased attention focused on the complex and coupled factors that control biocolloid (virus, protozoa, and bacteria) transport in fractured and porous media (Corapcioglu and Kim 1995; Sim and Chrysikopoulos 1995; Chrysikopoulos et al. 2000; Chrysikopoulos and Sim 1996; Stevik et al. 2004; Auset and Keller 2005; Anders and Chrysikopoulos 2005, 2009; Bradford et al. 2006; Brown and Abramson 2006; Maxwell et al. 2007; Masciopinto et al. 2008; Redman et al. 2004; Torkzaban et al. 2008; Kim et al. 2009; Syngouna and Chrysikopoulos 2010; Vasiliadou et al. 2011). Knowledge of the fundamental processes that control biocolloid transport is essential because it can aid to the development of appropriate groundwater

protection strategies and successful groundwater bioremediation technologies (Ginn et al. 2002; Tufenkji 2007).

The attachment of bacteria onto the solid matrix of subsurface formations is affected by the nature of bacterial as well as by the mineral surfaces (Powelson and Mills 2001; Becker et al. 2004; Foppen and Schijven 2005; Kim et al. 2008; Bolster et al. 2009; Vasiliadou and Chrysikopoulos 2011). However, the effects of interstitial fluid chemistry (Li and Logan 1999; Rogers and Logan 2000), pH and ionic strength (Fontes et al. 1991; Jewett et al. 1995; Choi et al. 2007; Kim et al. 2008, 2009) on biocolloid transport in porous media have been reported in the literature. Furthermore, previous studies have shown that the rate of bacteria attachment onto porous media can be enhanced (Camesano and Logan 1998; Camesano et al. 1999; Vasiliadou and Chrysikopoulos 2011) or hindered (Haznedaroglu et al. 2009; Torkzaban et al. 2010) by previously attached colloids.

Traditionally, the stability of colloids in natural environments is predicted by the Derjaguin–Landau–Verwey–Overbeek (DLVO) theory (Derjaguin and Landau 1941; Verwey and Overbeek 1948). Despite the fact that in subsurface formations both bacteria and the solid matrix are often negatively charged and thus the classical DLVO theory predicts the presence of a repulsive force between bacteria and solid surfaces, bacteria often attach onto the solid matrix. To resolve this discrepancy, numerous investigators have modified the DLVO theory to include factors not accounted for in the classical DLVO model. The extended-DLVO (XDLVO) theory includes the magnitude of the Lewis acid–base interaction (van Oss 1993; Yoon et al. 1997).

Most of the work to date on biocolloid transport in porous media has been aimed to examine biocolloid transport and interaction with granular materials (glass beads, soil, sand, and gravel) at the laboratory scale using columns (Gannon et al. 1991; Simoni et al. 1998; Camesano and Logan 1998; Hendry et al. 1999; Powelson and Mills 2001; Becker et al. 2004; Keller et al. 2004; Tong et al. 2005; Choi et al. 2007; Kim et al. 2008; Gargiulo et al. 2008; Harvey et al. 2010; Schinner et al. 2010; Syngouna and Chrysikopoulos 2011; Stumpp et al. 2011; Vasiliadou and Chrysikopoulos 2011). Relatively fewer biocolloid transport studies have been conducted at the field-scale (Harvey and Garabedian 1991; Duba et al. 1996; Harvey et al. 1993; Hubbard et al. 2001; Johnson et al. 2001; Zhang et al. 2001; Mailloux et al. 2003; Maxwell et al. 2007; Pavelic et al. 2007; Foppen et al. 2008) and just a few in 3-D pilot-scale model aquifers (Bales et al. 1995; Chrysikopoulos et al. 2010; Harvey and Garabedian 1991; Silliman et al. 2001).

In this study, the transport and attachment behavior of *P. putida* bacterial cells in a 3-D, water saturated, pilot-scale experimental aquifer packed with quartz sand was investigated. Emphasis was placed on whether the extended-DLVO approach can explain the observed attachment of *P. putida* onto quartz sand and on the simulation of bacteria transport in the 3-D pilot-scale aquifer, where field conditions are simulated much better than in packed columns.

2 Materials and Methods

2.1 Bacteria and Culture Preparation

The *P. putida* (ATCC17453) bacterial cells were cultured in 10 mL of nutrient broth (Laury Pepto Bios Broth 35.6 g/L, Biolife) over a period of 20 h and incubated at 30 °C in an orbital shaker (140 rpm) until an optical density at 600 nm (OD_{600}) of 0.5 Absorbance Units (AU)

was reached. Subsequently, 5 mL of culture were transferred to 250 mL of the same medium and incubated at 30 °C for 20 h (Choi et al. 2007; Kim et al. 2008; Rong et al. 2008; Vasiliadou and Chrysikopoulos 2011).

Bacterial cells in the late exponential growth phase ($OD_{600} = 0.9$) were harvested by centrifugation (10 min at $3{,}000 \times g$) and washed three times with sterile distilled water (sdH_2O) (Hendry et al. 1999; Choi et al. 2007; Vasiliadou and Chrysikopoulos 2011). Harvesting at the end of the logarithmic phase minimizes the potential for cell numbers increase during the transport experiments (Mills et al. 1994; Vasiliadou and Chrysikopoulos 2011). After the washing procedure, the bacteria were diluted in sdH_2O to obtain the desired experimental concentration of $1.8 \times 10^6 - 5.8 \times 10^8$ colony-forming units per milliter (CFU/mL), with a dry biomass concentration in the range of 10–658 mg of total cells/L. Following the work by Rong et al. (2008), the optical density of bacteria in sdH_2O was analyzed at a wavelength of 410 nm by a UV–Vis spectrophotometer (UV-1100, Hitachi). The absorbance of standard bacterial samples was measured at a wavelength of 410 nm, and the concentration of bacterial cells was calibrated using a standard curve of bacterial optical density based on dry weights. The standard curve (dry weights in mg/L versus bacterial optical density) was fitted with a linear type equation ($y = 189.11x$) with a correlation coefficient of $R^2 = 0.999$. This procedure was repeated three times to insure reproducibility.

Removing bacterial cells from growth media and resuspending them into sdH_2O could affect their motility, even alter their swimming speed. However, microscope examination verified that the bacterial cells were motile and still capable of growth as determined by plate counts on agar plates (Camesano and Logan 1998).

The zeta potential of the bacterial suspension at pH 7 in sdH_2O, measured by a zeta potential analyzer (ZetaSizer, Malvern Instruments Corporation), was estimated to be -44.2 ± 1.6 mV. The *P. putida* employed in this study was a rod-shaped bacterium with average length of $2.4 \pm 0.9\,\mu$m, average diameter of $0.9 \pm 0.1\,\mu$m, as determined from 50 SEM images of cells, and equivalent spherical diameter of $2.2 \pm 0.4\,\mu$m, as estimated by a ZetaSizer analyzer.

2.2 Quartz Sand

For this study, quartz sand (Filcom Filterzand & Grind) that passed the #20 sieve (850 μm) and retained on the #30 sieve (600 μm) was employed. Following the procedure outlined by Loveland et al. (1996) the surfaces of the quartz grains were prepared by washing 450 g of sand in 1,200 mL 0.1 M HNO_3 for 3 h in a 140 rpm orbital shaker. Next, the grains were rinsed three times with sdH_2O. Subsequently, the quartz grains were soaked in 0.1 M NaOH for 3 h, and rinsed repeatedly with sdH_2O until the pH reached the value of 7. The quartz grains were then dried in an oven at 105 °C. Finally, the sand as well as all of the glassware and materials used for this experimental study were sterilized in an autoclave at 121 °C for 20 min.

The quartz grains were too large for direct measurement of their zeta potential by the zeta potential analyzer. Therefore, a few quartz grains were crushed into a fine powder and then mixed with sdH_2O to form a sufficiently stable suspension that could be used for zeta potential measurement (Stephan and Chase 2001). The zeta potential of quartz grains stored in sdH_2O at pH 7 was determined to be -62.3 ± 3.5 mV.

2.3 Batch Experiments

Batch experiments were performed in order to measure the attachment of *P. putida* onto quartz grains as a function of bacterial concentration. Ten grams (10 g) of quartz sand were

mixed with 10 mL *P. putida* suspension in sdH_2O at pH 7 adjusted by adding appropriate amounts of 0.1 M NaOH and 0.1 M HNO_3 solution. The concentrations of the bacteria used were in the range of 10–658 mg of *P. putida*/L. Each mixture was gently shaken at 26 ± 1 °C for 100 min. Subsequently, the mixture was centrifuged at $2{,}000 \times g$ for 2 min.

Two sets of preliminary control experiments were conducted in centrifuge tubes in order to determine the most appropriate conditions for the separation of suspended bacteria from bacteria attached onto quartz grains. In the first set, only sand was placed in centrifuge tubes containing a cell-free solution of sdH_2O. In the second set, only aliquots of cell cultures were transferred in centrifuge tubes containing a sand-free solution of sdH_2O. The initial bacteria concentrations were measured for each control experiment. The tubes were centrifuged at different speeds for various time periods. It was observed that centrifugation at $2{,}000 \times g$ for 2 min was optimal, because for these conditions the supernatant contained all of the initial bacteria concentration and none of the sand particles.

The suspension of unattached bacteria in the supernatant was pipetted out and measured directly by spectrophotometry at 410 nm. The percentage of attached bacteria was determined by subtracting the mass of bacteria that remained in suspension from the initial mass of bacteria. The experimental data indicated that equilibrium was reached at approximately 60–80 min. Therefore, a contact time of 100 min was chosen for the equilibrium experiments, which were performed in triplicates to insure reproducibility.

2.4 Decay Rate of Suspended Bacteria

Batch experiments were designed to determine the decay rate of *P. putida* suspended in the aqueous phase, as a function of bacterial concentration and time. Three experiments were performed in 2 L closed flasks with different initial bacterial concentrations. The initial suspension concentrations were 56.1, 73.4, and 84.3 mg of *P. putida*/L sdH_2O at pH 7. Each bacterial suspension was continuously stirred at a constant rate of 500 rpm during all runs at 26 ± 1 °C. Samples were taken at preselected time intervals and analyzed immediately by spectrophotometry. All batch experiments were performed in triplicates.

2.5 Experimental Setup and Aquifer Characteristics

The experimental setup was designed following the study presented by Chrysikopoulos et al. (2000), Lee and Chrysikopoulos (2002, 2006), and Dela Barre et al. (2002). A schematic diagram of the 3-D, pilot-scale model aquifer used in this study is shown in Fig. 1, and a detailed sketch of the sampling plate is shown in Fig. 2. The model aquifer was contained within a rectangular glass tank with internal dimensions 120 cm length, 48 cm width, and 50 cm height. The glass thickness was 0.5 cm. The experimental aquifer was packed with 99.5 kg of quartz sand. The sand was packed into the model aquifer in 1–2 cm lifts to a total depth of about 14 cm, according to the procedure proposed by Chrysikopoulos et al. (2000). Each lift of sand was packed under a 5 cm water head. The dry bulk density of the sand and the aquifer porosity were determined to be $\rho_b = 1.63$ kg/L and $\theta = 0.38$, respectively. After the aquifer packing was completed, a steady sdH_2O flow was maintained through the model aquifer.

The aquifer sand was separated from the upstream and downstream clear wells by specially designed screens (Chrysikopoulos et al. 2000). Glass marbles with 1.9 cm diameter were added into the influent and effluent clear wells to balance the sand pressure exerted on the screens. A glass tube with 0.7 cm inner diameter was inserted in the center of each clear

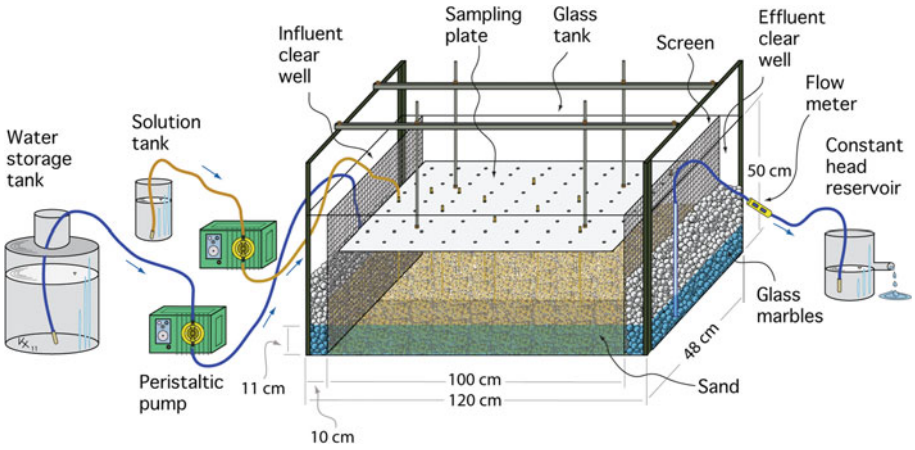

Fig. 1 Schematic diagram of the pilot-scale model aquifer

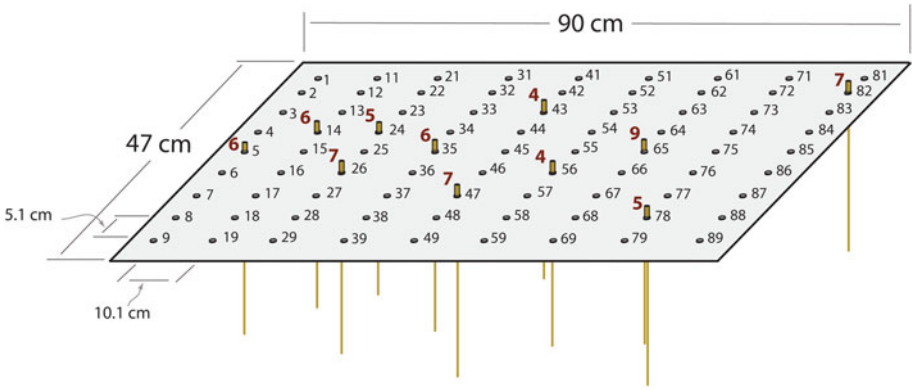

Fig. 2 Sampling plate and locations of the stainless steel sampling needles. The bold number in the upper left side of each sampling port indicates the needle placement depth in cm from the top of the aquifer ($z = 0$)

well to approximately 5.5 cm above the bottom of the aquifer. A peristaltic pump was used to pump sdH_2O from a flask through the glass tube into the influent clear well, while maintaining a constant head at the effluent clear well. The water elevation within the model aquifer was adjusted to a desired level of 11 cm by controlling the water elevation in the influent and effluent clear wells. Accurate determination of the volumetric flow rate through the model aquifer was obtained by a flowmeter attached onto the outlet tube, connecting the effluent clear well and the constant head reservoir. The water flow rate employed was 10 mL/min, which corresponded to an interstitial water velocity of $U = q/\theta = 3.1$ cm/h, where q is the Darcian flux. During each transport experiment, the pH of the influent and effluent were monitored, and the pH of the influent was maintained at pH 7 by adding appropriate amounts of 0.1 M NaOH. The pilot-scale model aquifer was placed in a room maintained at 26 ± 1 °C.

A sampling plate (see Fig. 2) was constructed from a $90 \times 47 \times 0.5$ cm Plexiglas sheet to allow precise positioning of sampling needles within the 3-D model aquifer. Two steel frames were placed on top of the glass tank to support the sampling plate (see Fig. 1). The sampling nodes consisted of nine columns by nine rows of 0.1 cm diameter holes (sampling

locations) positioned on a regular 10.1 × 5.1 cm^2 grid. Aqueous samples were collected from the experimental aquifer using 20 gauge, stainless steel luer hub needles (Hamilton, Reno, Nevada). It should be noted that a total of eleven needles were vertically inserted into the aquifer and their locations were indicated on the sampling plate. The designation of each sampling location (SL) was specified with a number located to the right of each SL, whereas the needle placement depth measured in centimeters from the top of the aquifer ($z = 0$) was indicated by a bold number at the left side of each SL (see Fig. 2).

2.6 Transport Experiments

A tracer experiment was conducted under steady flow conditions to characterize the 3-D model aquifer. Chloride, in the form of potassium chloride ($mw_{KCl} = 74.551$ g/mol, $\rho_{KCl} = 1.984$ g/cm^3), was chosen as the non-reactive tracer. It should be noted that alkali halides are the most commonly used salts for subsurface fluid tracing (Chrysikopoulos 1993). The non-reactive tracer solution (2 mS/cm) was prepared with 0.1 M KCl (12 mS/cm) in sdH_2O. After passing through the model aquifer 3 PV (1 PV ≈ 19.8 L ≈ 33 h) of sdH_2O, a source solution containing 850 mg/L Cl^- was injected into the model aquifer via a peristaltic pump through a needle located at the pre-selected SL 5 (see Fig. 2). Note that the injected tracer source concentration should be low enough to avoid any density effects and gravity segregation, yet high enough to insure tracer detection by the analytical technique of choice. Preliminary experiments showed that for the relatively low tracer concentration used in this study no significant gravity effects occurred in the model aquifer, while tracer detection was insured. The tracer (1,152 mL) was injected into the model aquifer with a constant and relatively slow injection rate (0.4 mL/min) over a pulse period of 48 h, so that the flow field within the model aquifer was not disturbed. As soon as all tracer samples were collected, sdH_2O was pumped into the influent clear well to completely remove the tracer from the experimental aquifer.

Following the tracer experiment, a bacterial suspension of 75 mg of total cells/L were injected into the model aquifer through the SL 5 at an injection rate of 0.4 mL/min over a time period of 48 h. Throughout the injection period, the bacterial suspension in the storage flask was maintained at 75 mg of total cells/L by replacing the bacterial suspension with new as needed. After the bacterial injection was completed, sdH_2O was pumped into the influent clear well of the aquifer until the bacterial concentration in the samples collected was completely diminished. Periodically, 0.4 mL of the interstitial liquid was collected from several sampling locations. Because the fluid within the sampling needles does not equilibrate fast enough with the local solution within the model aquifer, 0.1 mL of interstitial fluid was purged and discarded from the sampling needle just before each sample collection (Chrysikopoulos et al. 2000). All samples were collected into borosilicate test tubes. Chloride concentrations were measured using ion chromatography (DIONEX500, Sunnyvale, CA) and bacterial concentrations using UV–vis spectrophotometry (UV-1100, Hitachi).

3 Mathematical Modeling

The transport of dissolved/suspended species in saturated, homogeneous porous media, accounting for 3-D hydrodynamic dispersion in a uniform flow field, nonequilibrium sorption/attachment, and first-order decay of liquid phase and sorbed species with different decay rates, is governed by the following partial differential equation (Sim and Chrysikopoulos 1998, 1999):

$$\frac{\partial C(t,x,y,z)}{\partial t} + \frac{\rho_b}{\theta}\frac{\partial C^*(t,x,y,z)}{\partial t} - D_x\frac{\partial^2 C(t,x,y,z)}{\partial x^2} - D_y\frac{\partial^2 C(t,x,y,z)}{\partial y^2} - D_z\frac{\partial^2 C(t,x,y,z)}{\partial z^2} + U\frac{\partial C(t,x,y,z)}{\partial x} + \lambda C(t,x,y,z) + \lambda^*\frac{\rho_b}{\theta}C^*(t,x,y,z) = F(t,x,y,z) \quad (1)$$

where C is the concentration of species dissolved/suspended in the aqueous phase; C^* is the concentration of species attached onto the solid phase; U is the average interstitial velocity; D_x, D_y, and D_z are the longitudinal, lateral, and vertical hydrodynamic dispersion coefficients, respectively; t is time; x, y, and z are the spatial coordinates in the longitudinal, lateral, and vertical directions respectively; ρ_b is the bulk density of the solid matrix; θ is the porosity of the porous medium; λ is the decay rate of liquid-phase species; λ^* is the decay rate of species sorbed or attached onto the solid matrix; and F is a general form of the source configuration.

The dispersion coefficients are defined as (Bear and Verruijt 1987):

$$D_x = \alpha_L U + \mathcal{D}_e \quad (2)$$

$$D_y = \alpha_{Ty} U + \mathcal{D}_e \quad (3)$$

$$D_z = \alpha_{Tz} U + \mathcal{D}_e \quad (4)$$

where α_L, α_{Ty}, and α_{Tz} are the dispersivities in the longitudinal, lateral, and vertical directions, and $\mathcal{D}_e = \mathcal{D}_{AB}/\tau^*$ is the effective molecular diffusion coefficient ($\tau^* \geq 1$ is the tortuosity coefficient, and $\mathcal{D}_{AB}$ is the molecular diffusion coefficient).

The accumulation of bacterial cells onto the solid matrix of the aquifer (quartz sand) is described by the nonequilibrium equation (Sim and Chrysikopoulos 1998, 1999):

$$\frac{\rho_b}{\theta}\frac{\partial C^*(t,x,y,z)}{\partial t} = k_c C(t,x,y,z) - k_r\frac{\rho_b}{\theta}C^*(t,x,y,z) - \lambda^*\frac{\rho_b}{\theta}C^*(t,x,y,z) \quad (5)$$

where k_c is the attachment rate coefficient of species onto quartz sand, and k_r is the detachment rate coefficient of species from quartz sand.

The initial condition and the appropriate boundary conditions for the aquifer model employed in this study are as follows:

$$C(0,x,y,z) = 0 \quad (6)$$

$$C(t,0,y,z) = 0 \quad (7)$$

$$\frac{\partial C(t,L_x,y,z)}{\partial x} = 0 \quad (8)$$

$$\frac{\partial C(t,x,0,z)}{\partial y} = \frac{\partial C(t,x,L_y,z)}{\partial y} = 0 \quad (9)$$

$$\frac{\partial C(t,x,y,0)}{\partial z} = \frac{\partial C(t,x,y,L_z)}{\partial z} = 0 \quad (10)$$

where L_x, L_y, and L_z are the dimensions of the porous medium in the x-, y-, and z-direction, respectively. Condition (6) establishes that there is no initial solute concentration within the 3-D porous medium. The zero-concentration condition (7) implies that no solutes or biocolloids are entering the porous medium from the influent clear well. The downstream boundary condition (8) preserves concentration continuity at the effluent clear well. Conditions (9) and (10) imply that there is no solute or biocolloid flux across the lateral and vertical boundaries of the 3-D porous medium.

The molecular diffusion coefficient of a solute can be estimated (in units of cm^2/s), using the Wilke–Chang relationship (Wilke and Chang 1955):

$$\mathcal{D}_{AB} = 7.4 \times 10^{-8} \frac{\left(\psi_B \, mw_B\right)^{1/2} T}{\mu_B \, V_A^{0.6}} \tag{11}$$

where A is the solute; B is the solvent (water); $\psi_B = \psi_{H_2O} = 2.6$ is an association parameter for solvent B (Bird et al. 2002); $\mu_B = \mu_w = 0.890 \times 10^{-3}$ (N s)/m^2 = 0.89 cp is the water viscosity at 25 °C in units of centipoises (1 cp = 0.001 (N s)/m^2), $mw_B = 18$ g/mol is the molecular weight of water, $T = 298$ K is the absolute temperature of the interstitial fluid, and $V_A = mw_A/\rho_A$ is the molar volume of solute A measured in cm^3/mol. Also, for suspended particles of finite size (i.e., biocolloids) the molecular diffusion coefficient is specified by the Stokes–Einstein diffusion equation (Russel et al. 1989):

$$\mathcal{D}_{AB} = \frac{k_B T}{3\pi \mu_B d_p} \tag{12}$$

where d_p is the particle diameter, and $k_B = 1.38 \times 10^{-23}$ J/K is the Boltzmann constant.

Several tortuosity models based on molecular diffusivity and electrical resistivity are available in the literature (Garrouch et al. 2001). In this study, the tortuosity model introduced by Bruggeman (1935) is employed:

$$\tau^* = \theta^{1-\alpha} \approx \frac{1}{\sqrt{\theta}} \tag{13}$$

where α is the dimensionless Bruggeman exponent, which frequently is employed with the value of $\alpha \approx 1.5$ (Pisani 2011).

The numerical solution to Eqs. (1) through (10) was obtained by the fully implicit finite-difference method, which is known to be stable for any spatial (Δx, Δy, Δz) and temporal steps (Δt). The advection term was approximated with the central difference scheme, which is free from numerical dispersion. To avoid artificial oscillations, which could occur in the presence of sharp concentration fronts, the Peclet number ($Pe = U \, \Delta x/D_x$) was kept smaller than 2 (Huyakorn and Pinder 1983). Furthermore, to avoid numerical dispersion, which can artificially be created by the approximation of the time derivative, the dimensionless Courant number, ($N_{Cr} = U \, \Delta t/\Delta x$) was restricted to be lower than one (Zheng and Bennet 1995). The numerical solution was tested against the analytical solution provided by Sim and Chrysikopoulos (1999) for the case of a 3-D porous medium with finite thickness. Note that the singularity associated with the source cell concentration was also included in the comparison. Figure 3 shows very good agreement between the numerical and analytical solution everywhere except at the source location. The discrepancy at the source point occurs because the analytical solution assumes a point source, whereas for the numerical solution the source is the volume of a discretization unit cell ($\Delta x \times \Delta y \times \Delta z$), and the existence of a sharp concentration front. This discrepancy can be reduced by increasing the number of discretization unit cells n_x, n_y, and n_z in the x-, y-, and z-direction, respectively. All model simulations presented in this work were conducted for $L_x = 90$ cm, $L_y = 47$ cm, $L_z = 11$ cm, $n_x = 151$, $n_y = 85$, $n_z = 19$, and $\Delta t = 0.125$ h. Furthermore, all fittings of the transport model to the experimental data were obtained by a model-independent parameter estimation software PEST (2010), which employs the Gauss–Marquardt–Levenberg algorithm to determine the optimal set of model parameters.

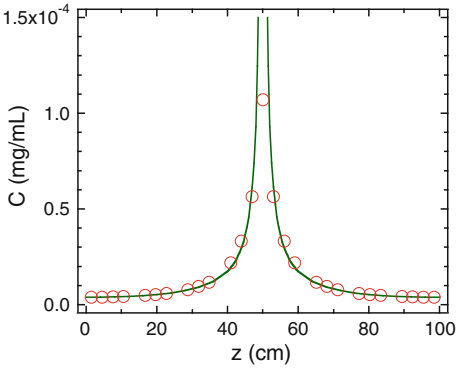

Fig. 3 Comparison between analytical and numerical solutions at a specific line $(x, y, z) = (200, 250\text{ cm}, z)$ and $t = 5$ d within a 3-D aquifer with finite thickness $H = 100$ cm for a point source located at $x = 200$ cm, $y = 250$ cm, $z = 50$ cm. Here, $F = 4$ g/(cm^3 d), $D_x = 1,950$ cm^2/d, $D_y = D_z = 1,450$ cm^2/d, $U = 15$ cm/d, $\lambda = \lambda^* = 0\,\text{d}^{-1}$ $k_c = 0.72\,\text{d}^{-1}$, $k_r = 0.4\,\text{d}^{-1}$, $\theta = 0.25$, $L_x = L_y = 500$ cm, $L_z = H = 100$ cm, $n_x = n_y = 71$, $n_z = 33$, and $\Delta t = 0.25$ d

4 Moment Analysis

The tracer and bacteria concentrations obtained at various sampling locations were analyzed by the absolute temporal moments:

$$m_n(x) = \int_0^\infty t^n C(x,t)\,\mathrm{d}t \tag{14}$$

where the subscript $n = 0, 1, 2, \ldots$ indicates the order of the moment. The zeroth absolute temporal moment, m_0, quantifies the total mass in the concentration distribution curve; the first absolute moment, m_1, describes the mean residence time; and second absolute temporal moment, m_2, describes the degree of spreading of the concentration distribution curve. Also, the normalized temporal moments are defined as (James and Chrysikopoulos 2011):

$$M_n(x) = \frac{m_n(x)}{m_0(x)} = \frac{\int_0^\infty t^n C(x,t)\,\mathrm{d}t}{\int_0^\infty C(x,t)\,\mathrm{d}t} \tag{15}$$

The first normalized temporal moment, M_1, characterizes the center of mass of the concentration distribution curve and defines the average velocity. The second normalized temporal moment, M_2, characterizes the spreading of the concentration distribution curve. Worthy to note is that the ratio $M_{1(b)}/M_{1(t)}$ indicates the degree of velocity enhancement of bacteria relative to the conservative tracer. If this ratio is less than one, there exists velocity enhancement of bacteria transport. If this ratio is >1 there exists bacteria retardation. One frequently employed method for normalized temporal-moment estimation of experimental or distinct data applies the unbiased trapezoidal integration scheme as follows (Haas 1996):

$$M_n(x) = \frac{\sum_{j=2}^{\omega} \frac{1}{2}\left(t_j^n C_j + t_{j-1}^n C_{j-1}\right)\left(t_j - t_{j-1}\right)}{\sum_{j=2}^{\omega} \frac{1}{2}\left(C_j + C_{j-1}\right)\left(t_j - t_{j-1}\right)} \tag{16}$$

where $C_j = C(x, t_j)$ is the solute or bacterial concentration at time $t = t_j$, and ω is the number of time steps.

5 Bacteria–Quartz Sand Interactions

Based on the classical DLVO theory, the total interaction energy between two surfaces is determined by the van der Waals, Φ_{vdW}, double layer, Φ_{dl}, and Born, Φ_{Born}, potential energies (Loveland et al. 1996):

$$\Phi_{\mathrm{DLVO}}(h) = \Phi_{\mathrm{vdW}}(h) + \Phi_{\mathrm{dl}}(h) + \Phi_{\mathrm{Born}}(h) \tag{17}$$

where h is the separation distance between the approaching surfaces. For the case of two approaching surfaces, one with spherical and the other with planar geometries (sp for sphere–plate), the $\Phi_{\mathrm{vdW-sp}}$ interactions were calculated with the following expression (Gregory 1981):

$$\Phi_{\mathrm{vdW-sp}}(h) = -\frac{A_{123} r_{\mathrm{p}}}{6h}\left[1 + \left(\frac{14h}{\lambda_w}\right)\right]^{-1} \tag{18}$$

where A_{123} is the combined Hamaker constant for microscopic bodies of composition "1" and "3" in medium "2", $\lambda_{\mathrm{w}} \approx 10^{-7}\ m$ is the characteristic wavelength of the sphere–plate interactions, and r_{p} is the radius of the bacterial cell. The $\Phi_{\mathrm{dl-sp}}$ for sphere–plate interactions were calculated with the expression (Hogg et al. 1966)

$$\Phi_{\mathrm{dl-sp}}(h) = \pi \varepsilon_r \varepsilon_0 r_{\mathrm{p}}\left[2\Psi_{\mathrm{p}}\Psi_{\mathrm{s}} \ln\left(\frac{1 + e^{-\kappa h}}{1 - e^{-\kappa h}}\right) + \left(\Psi_{\mathrm{p}}^2 + \Psi_{\mathrm{s}}^2\right)\ln\left(1 - e^{-2\kappa h}\right)\right] \tag{19}$$

where $\varepsilon_r = \varepsilon/\varepsilon_0$ is the dimensionless relative dielectric constant of the suspending liquid, ε is the dielectric constant of the suspending liquid, ε_0 is the permittivity of free space, ψ_{p} is the surface potential of the biocolloid particle, ψ_{s} is the surface potential of the collector surface (plate), and κ is the inverse of the diffuse layer thickness, known as the Debye–Huckel parameter:

$$\kappa = \left[\frac{2I_{\mathrm{s}} N_{\mathrm{A}} 1{,}000 e^2}{\varepsilon_r \varepsilon_0 k_{\mathrm{B}} T}\right]^{1/2} \tag{20}$$

where I_{s} is the ionic strength, $N_{\mathrm{A}} = 6.02 \times 10^{23}$ molecules/mole is Avogadro's number, and $e = -1.602 \times 10^{-19}$ C is the charge of an electron. In this study, the measured zeta potentials, ζ, are used instead of the surface potentials (Chrysikopoulos and Syngouna 2012). The $\Phi_{\mathrm{Born-sp}}$ for sphere–plate was estimated by the relationship (Ruckenstein and Prieve 1976)

$$\Phi_{\mathrm{Born-sp}}(h) = \frac{A_{123}\,\sigma_{\mathrm{Born}}^6}{7560}\left[\frac{8r_{\mathrm{p}} + h}{(2r_{\mathrm{p}} + h)^7} + \frac{6r_{\mathrm{p}} - h}{h^7}\right] \tag{21}$$

where σ_{Born} is the Born collision parameter. For the commonly used value of $\sigma_{\mathrm{Born}} = 5$ Å (Ruckenstein and Prieve 1976), the resulting acceptable minimum separation distance, at $h = h_{\mathrm{o}}$, i.e., at "contact", is estimated to be $h_{\mathrm{o}} \approx 2.5$ Å $= 0.25$ nm.

For the case of sphere–sphere (ss) particle geometries, the Φ_{vdW-ss} interactions were calculated with the following expression (Feke et al. 1984; Ryan and Gschwend 1994)

$$\Phi_{vdW-ss}(h) = -\frac{A_{123}}{12}\left\{\frac{R_p}{\xi^2+\xi R_p+\xi}+\frac{R_p}{\xi^2+\xi R_p+\xi+R_p}+2\ln\left[\frac{\xi^2+\xi R_p+\xi}{\xi^2+\xi R_p+\xi+R_p}\right]\right\} \tag{22}$$

where

$$R_p = \frac{r_{p2}}{r_{p1}} \tag{23}$$

$$\xi = \frac{h}{r_{p1}} \tag{24}$$

r_{p1} is the radius of the spherical colloid particle 1, and r_{p2} is the radius of the spherical colloid particle 2 (usually $r_{p1} \le r_{p2}$). The Φ_{dl-ss} for sphere–sphere interactions were calculated with the expression (Hogg et al. 1966)

$$\Phi_{dl-ss}(h) = \pi\varepsilon_r\varepsilon_0\frac{r_{p1}r_{p2}}{(r_{p1}+r_{p2})}\left[2\Psi_{p1}\Psi_{p2}\ln\left(\frac{1+e^{-\kappa h}}{1-e^{-\kappa h}}\right)+\left(\Psi_{p1}^2+\Psi_{p2}^2\right)\ln\left(1-e^{-2\kappa h}\right)\right] \tag{25}$$

where ψ_{p1} is the surface potential of the colloid, and ψ_{p2} is the surface potential of the second sphere. The $\Phi_{Born-ss}$ for sphere–sphere interactions were estimated with the relationship (Feke et al. 1984; Ryan and Gschwend 1994):

$$\begin{aligned}\Phi_{Born-ss}(h) = \frac{A_{123}}{7560\xi}\left(\frac{\sigma_{Born}}{r_{p1}}\right)^2\Bigg[&\frac{-4\xi^2-14(R_p-1)\xi-6\left(R_p^2-7R_p+1\right)}{(2\xi-1+R_p)^7}\\ &+\frac{-4\xi^2+14(R_p-1)\xi-6\left(R_p^2-7R_p+1\right)}{(2\xi+1-R_p)^7}\\ &+\frac{4\xi^2+14(R_p-1)\xi+6\left(R_p^2+7R_p+1\right)}{(2\xi+1+R_p)^7}\\ &+\frac{4\xi^2-14(R_p-1)\xi+6\left(R_p^2+7R_p+1\right)}{(2\xi-1-R_p)^7}\Bigg]\end{aligned} \tag{26}$$

In this study, the combined Hamaker constant $A_{123} = 6.5\times10^{-21}$ J reported by Redman et al. (2004) for *E.coli* K12 strain and ultrapure quartz sand interactions was used for the system bacteria cells–water–quartz sand, and the value of $A_{121} = 7.5\times10^{-20}$ J reported by Kim et al. (2010) for *E.coli* O157:H7/pGFP strain 72 was used for the system bacteria-water-bacteria.

Discrepancies between experimental data and DLVO theory frequently occur due to additional energies, namely hydration pressure, hydrogen bonding forces, hydrophobic effects, disjoining pressure, structural forces, and Lewis acid–base forces (Israelachvili 1992; van Oss 1994; Swanton 1995; Bergendahl and Grasso 1999). These forces are attractive or repulsive and they are known to be sensitive to adsorption of ions or molecules at the interface. The non-DLVO short-range repulsive forces have been termed hydration forces, while longer-range attractive forces between hydrophobic bodies have been considered hydrophobic interactions. van Oss (1993) calculated the non-DLVO forces that arise from Lewis acid–base electron

donor–acceptor interactions between surfaces, adsorbed species, and the solvent. The incorporation of additional energies of interaction into the simple DLVO model is currently known as the extended-DLVO or XDLVO theory, which is considered as the sum of the classical DLVO, Φ_{DLVO}, and Lewis acid–base, Φ_{AB}, interaction energy over a separation distance, h, between two approaching surfaces (Bergendahl and Grasso 1999):

$$\Phi_{\mathrm{XDLVO}}(h) = \Phi_{\mathrm{DLVO}}(h) + \Phi_{\mathrm{AB}}(h) \tag{27}$$

The Lewis acid–base interaction energy, Φ_{AB}, decays exponentially with distance (van Oss 1994). In the case of sphere–plate $\Phi_{\mathrm{AB-sp}}$ interactions were calculated with the following relation (van Oss 1994; van Oss and Giese 2004):

$$\Phi_{\mathrm{AB-sp}}(h) = 2\pi r_{\mathrm{p}} \lambda_{\mathrm{AB}} \Phi_{\mathrm{AB}(h=h_{\mathrm{o}})} \exp\left[\frac{h_0 - h}{\lambda_{\mathrm{AB}}}\right] \tag{28}$$

and for the case of sphere–sphere $\Phi_{\mathrm{AB-ss}}$ interactions with the following relation

$$\Phi_{\mathrm{AB-ss}}(h) = 2\pi \frac{r_{\mathrm{p1}} r_{\mathrm{p2}}}{r_{\mathrm{p1}} + r_{\mathrm{p2}}} \lambda_{\mathrm{AB}} \Phi_{\mathrm{AB}(h=h_{\mathrm{o}})} \exp\left[\frac{h_0 - h}{\lambda_{\mathrm{AB}}}\right] \tag{29}$$

where $\Phi_{\mathrm{AB}(h=h_{\mathrm{o}})}$ is the Lewis acid–base free energy of interaction between two surfaces at $h = h_{\mathrm{o}}$ (i.e., at "contact"), λ_{AB} is the decay (Debye) length of water. For this work, it was assumed that $\lambda_{\mathrm{AB}} = 1$ nm (van Oss et al. 1990), and $h_{\mathrm{o}} = 0.25$ nm. Currently, there are two approaches for the estimation of $\Phi_{\mathrm{AB}(h=h_{\mathrm{o}})}$. The first approach is theoretical, developed by van Oss (1994) and it is based on the surface tension electron-acceptor and -donor parameters of the individual materials; whereas, the second approach is empirical, developed by Yoon et al. (1997) and it is based on the determination of the degree of hydrophobicity using water contact angles. Bergendahl and Grasso (1999) compared the two methods and found that they lead to quite similar results. In this study, the $\Phi_{\mathrm{AB}(h=h_{\mathrm{o}})}$ is estimated by the empirical approach developed by Yoon et al. (1997):

$$\Phi_{\mathrm{AB}(h=h_{\mathrm{o}})} = -\frac{K_{123}}{2\pi h_0 \lambda_{\mathrm{AB}}} \tag{30}$$

where K_{123} is the hydrophobic force constant, which can be predicted by the following empirical relationship

$$\log K_{123} = -7.0\left(\frac{\cos\beta_1 + \cos\beta_3}{2}\right) - 18.0 \tag{31}$$

where β_1 and β_3 are the water contact angles of materials "1" and "3", respectively. Contact angles are used to determine the hydrophobicity of bacteria and quartz sand surfaces. Note that different *P. putida* bacterial strains display considerable diversity in cell surface properties (van der Mei et al. 1998), and thus contact angles published in the literature should be employed with caution. The contact angles used in this study are: $\beta = 49 \pm 2°$ for *P. putida*, based on a model *P. putida* strain with identical growth and purification procedures to the strain employed here (Aronov et al. 2008), and $\beta = 70.8 \pm 0.5°$ for clean quartz sand, based on measurements of purified silica sand under very similar experimental conditions (Chen and Zhu 2005).

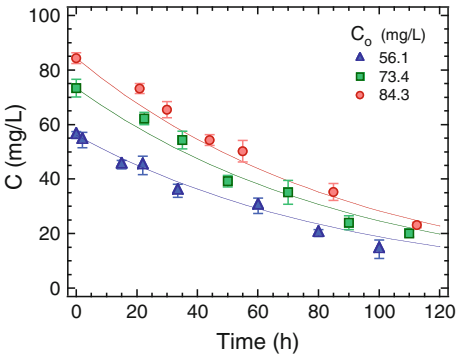

Fig. 4 Kinetics of *P. putida* decay in the aqueous phase for three different initial bacterial concentrations (*symbols*) and fitted first-order model (*curves*) (here $R^2 = 0.981$)

6 Results and Discussion

The *P. putida* decay data shown in Fig. 4 were adequately fitted by the following first-order relationship (Chrysikopoulos and Vogler 2004):

$$\frac{dC\,(t)}{dt} = -\lambda C\,(t) \tag{32}$$

where $\lambda = 0.0109\,h^{-1}$ is the fitted decay coefficient for *P. putida* suspended in the aqueous phase. The attachment of *P. putida* onto the sand was fitted with a linear isotherm.

Theoretically, as illustrated in Fig. 5, a DLVO interaction energy profile is characterized by a deep energy "well", which appears at relatively small separation distances and it is known as the primary minimum, Φ_{min1}, the energy barrier to attachment and detachment known as the primary maximum, Φ_{max1}, and a shallow energy "well" at relatively large separation distances known as the secondary minimum, Φ_{min2}. The interaction energy profile between *P. putida* and quartz sand was calculated using the classical DLVO theory as applied to the sphere–plate model for the experimental conditions of this study (pH 7, $I_s = 10^{-4}$M) and it is shown in Fig. 6. The Φ_{dl-sp} values were calculated with Eq. (19) using electrokinetic zeta potentials instead of surface potentials. Figure 6 suggests that the experimental conditions of this study are highly unfavorable for irreversible bacteria attachment in the primary minimum Φ_{min1}. Note that the height of the energy barrier, Φ_{max1}, is 3,693 k_BT, and the secondary energy minimum, Φ_{min2}, is $-0.01\ k_BT$, which is much smaller than the average Brownian kinetic energy of 1.5 k_BT and appears at the relatively long separation distance of $h \approx 450$ nm. Under these unfavorable conditions, *P. putida* cells approaching quartz sand grains experience an attractive force due to the Φ_{min2} energy well before encountering the repulsive Φ_{max1}. Therefore, attachment of *P. putida* at Φ_{min2} is possible if the sum of the particle Brownian kinetic energy and the fluid drag force are small enough to keep a particle in the energy well. Worthy to note is that taking into account particle deposition at Φ_{min2}, significantly improves the agreement between theory and experimental data (Redman et al. 2004). Moreover, for the experimental conditions of this study, reversible *P. putida* attachment onto quartz sand could occur due to polymer bridging (Jucker et al. 1998; Liu et al. 2007) and surface roughness of the quartz sand, which may provide hydrodynamically favorable attachment sites (Redman et al. 2001; Tufenkji et al. 2004; Bradford et al. 2007; Torkzaban et al. 2008).

The $\Phi_{DLVO-sp}$, Φ_{AB-sp}, and $\Phi_{XDLVO-sp}$ predicted profiles for *P. putida* and quartz sand, as applied to the sphere–plate model, are shown in Fig. 7 for the experimental conditions of this study (pH 7, $I_s = 10^{-4}$ M) in order to evaluate the relative contribution of the Lewis

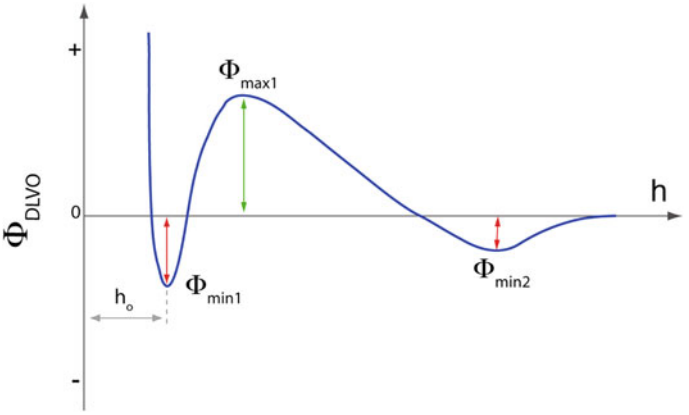

Fig. 5 Definition sketch of the interaction energy between two approaching surfaces versus their separation distance, showing the primary minimum, Φ_{min1} (deep energy "well"), the primary maximum, Φ_{max1} (energy barrier to attachment and detachment), and the secondary minimum, Φ_{min2} (shallow energy "well"), and the minimum separation distance h_o

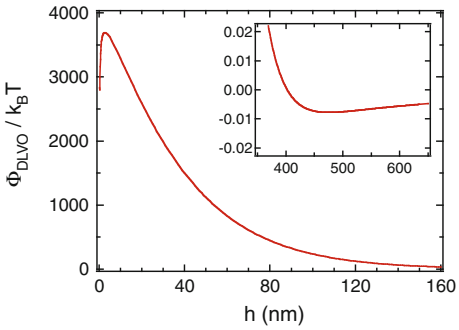

Fig. 6 Predicted DLVO interaction energy profile for *P. putida* with quartz sand as a function of separation distance for the experimental conditions, using sphere-plate approximation. The figure *inset* highlights the corresponding secondary energy minimum, Φ_{min2}

acid–base interaction energy to the XDLVO. The various Φ_{max1}, Φ_{min1}, and Φ_{min2} calculated values are listed in Table 1. In order to quantify the affinity of *P. putida* to quartz sand, the Lewis acid–base free energy of interaction was evaluated at $h_0 = 0.25$ nm with the empirical relationship (28) and it was found to be negative and equal to $\Phi_{AB(h=h_o)} = -141.5$ mJ/m^2, demonstrating relatively strong adhesion potential of *P. putida* onto quartz sand. Clearly, the Φ_{AB-sp} hydrophobic interaction energy profile significantly influences the $\Phi_{XDLVO-sp}$ profile. Worthy to note is that the Φ_{AB-sp} component of the XDLVO theory describes attractive hydrophobic interactions and repulsive hydration effects, which are at least an order of magnitude stronger than van der Waals interactions (van Oss 1989). It is evident from Fig. 7 that the acid–base interactions are only affecting the energy curve at small separation distances near the primary minimum, but not at the secondary minimum. Therefore, the acid–base interactions were involved in the attachment of *P. putida* at the primary minimum. Because *P. putida* cells and quartz sand were both negatively charged, they were subjected to repulsive electrostatic interactions at separation distances of several tens of nanometers. However, local charge heterogeneities and surface asperities of the quartz sand that induce attractive interactions with *P. putida* could form localized reduction of the total repulsive interaction energy. Consequently, *P. putida* cells attached at Φ_{min2} could transit more easily between Φ_{min2} and Φ_{min1} (Kuznar and Elimelech 2007). When *P. putida* cells overcome the repulsive

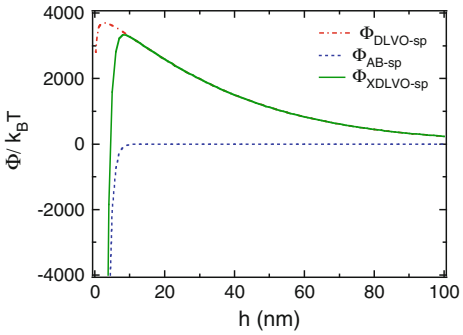

Fig. 7 Predicted sphere–plate $\Phi_{DLVO-sp}$, Φ_{AB-sp}, and $\Phi_{XDLVO-sp}$ interaction energy profiles for *P. putida* and quartz sand, as a function of separation distance, for the experimental conditions

Table 1 Calculated parameters defining the interaction energy between *P. putida* and quartz sand using both DLVO and XDLVO theories for the experimental conditions (pH 7, $I_s = 10^{-4}$ M)

Colloid stability theory	Interaction between *P. putida* and quartz sand					
	h (nm)	$\Phi_{min1}(k_BT)$	h (nm)	$\Phi_{max1}(k_BT)$	h (nm)	$\Phi_{min2}(k_BT)$
DLVO	na[a]	na[a]	3	3693	474	−0.01
XDLVO	0.25	−231457	8	3326	474	−0.01

[a] There is no primary minimum depth, Φ_{min1} can not be calculated

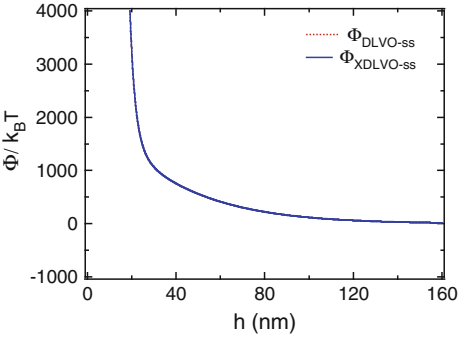

Fig. 8 Predicted sphere–sphere $\Phi_{DLVO-ss}$, and $\Phi_{XDLVO-ss}$ interaction energy profiles for *P. putida–P. putida* cells as a function of separation distance, for the experimental conditions

barrier and get closer to quartz sand, van der Waals and Lewis acid–base interactions begin to dominate. At the equilibrium distance of $h_0 = 0.25$ nm where physical contacts occur, electrostatic interactions can be ignored because van der Waals and Lewis acid–base interactions provide the driving force for *P. putida* attachment onto the quartz sand (van Oss 1994). The XDLVO theory qualitatively predicts better the experimental *P. putida* attachment results than the classical DLVO theory, but the information gained should be used with caution in complex subsurface environments.

The $\Phi_{DLVO-ss}$ and $\Phi_{XDLVO-ss}$ predicted profiles for *P. putida–P. putida* interactions, as applied to the sphere–sphere model, are shown in Fig. 8 for the experimental conditions of this study (pH 7, $I_s = 10^{-4}$ M) in order to evaluate the possibility of bacterial aggregation. Clearly, both the classical DLVO and the XDLVO theory suggest that, no coagulation between like particles is expected to occur under the experimental conditions.

In view of Eq. (11), the molecular diffusion of the tracer is estimated to be $\mathcal{D}_{AB(KCl)} = 1.924 \times 10^{-5}$ cm^2/s, and from Eq. (12) the molecular diffusion of the bacteria is estimated

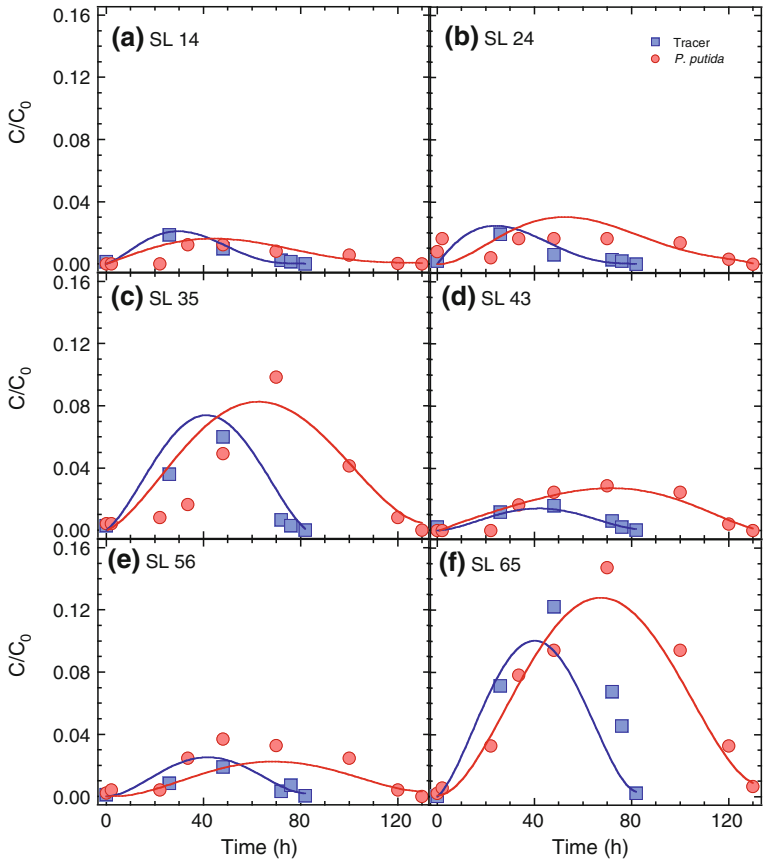

Fig. 9 Experimental data (*symbols*) and fitted model simulations (*curves*) for transport of the chloride tracer (*squares*) and *P. putida* bacteria (*circles*) as a function of time at several sampling locations within the 3-D bench scale experimental aquifer

to be $\mathcal{D}_{\mathrm{AB}(P.\ putida)} = 2.228 \times 10^{-9}\ \mathrm{cm}^2/\mathrm{s}$. Also, in view of Eq. (13), the tortuosity is estimated to be $\tau^* = 1.6$. Therefore, the effective molecular diffusion for the tracer is $\mathcal{D}_{\mathrm{e(KCl)}} = 1.203 \times 10^{-5}\mathrm{cm}^2/\mathrm{s}$, and for the bacteria is $\mathcal{D}_{\mathrm{e}(P.putida)} = 1.393 \times 10^{-9}\ \mathrm{cm}^2/\mathrm{s}$.

The normalized chloride concentrations as a function of time, at various locations within the 3-D bench scale experimental aquifer, are presented in Fig. 9. The tracer data were fitted with the transport model (1–10), assuming that the parameters k_c, k_r, λ, λ^* are equal to zero, the unknown hydrodynamic dispersion coefficients D_x, $D_y = D_z$, and the interstitial velocity U were estimated. The assumed relationships for the transverse and vertical dispersion coefficients were imposed by the need to reduce the number of unknown parameters to be fitted. It is worthy to note that having to fit more than three parameters simultaneously leads to non-unique set of estimated parameters. All fitted and experimentally determined parameter values are listed in Table 2. The desired model aquifer dispersivities were determined to be: $\alpha_{\mathrm{L}} = 8.46$ cm, $\alpha_{Ty} = \alpha_{Tz} = 0.45$ cm. Figure 10 shows the tracer concentrations observed at sampling locations 14, 24, and 26, in appropriate vertical $y - z$ planes at two different times together with the corresponding concentration contours predicted by the numerical transport model using the best-fitted D_x, D_y, D_z and U values. Similarly, Fig. 11 shows the tracer

Table 2 Model parameters values for tracer and bacteria transport experiments

Parameter	Status	KCl	Status	*P. putida*
D_x	Fitted	$26.3 \pm 10\,\text{cm}^2/\text{h}$	Fitted	$14.1 \pm 7.91\,\text{cm}^2/\text{h}$
$D_y = D_z$	Fitted	$1.46 \pm 0.84\,\text{cm}^2/\text{h}$	Fitted	$0.97 \pm 0.37\,\text{cm}^2/\text{h}$
α_x	Estimated	8.46 cm	Estimated	4.54 cm
$\alpha_{Ty} = \alpha_{Tz}$	Estimated	0.45 cm	Estimated	0.31 cm
F	Fixed	20.4 mg/(h cm^3)	Fixed	1.8 mg/(h cm^3)
k_c	Fixed	0 1/h	Fixed	0.78 1/h
k_r	Fixed	0 1/h	Fitted	0.26 ± 0.14 1/h
U	Fitted	3.1 ± 1.94 cm/h	Fixed	3.1 cm/h
θ	Fixed	0.38	Fixed	0.38
λ	Fixed	0 1/h	Fixed	0.0109 1/h
λ^*	Fixed	0 1/h	Fixed	0.00545 1/h
ρ_b	Fixed	1.63 kg/L	Fixed	1.63 kg/L

concentrations observed at sampling locations 14, 24, 35, and 78, in appropriate vertical $x - y$ planes at two different times. It should be noted that the solid circles in Figs. 10 and 11 represent sampling locations and the bold number next to each sampling location represents the corresponding chloride concentration. Figures 10 and 11 show relatively good agreement between the observed chloride concentrations and the numerical solution.

The normalized *P. putida* concentrations as a function of time, at various locations within the 3-D bench scale experimental aquifer, are presented in Fig. 9. The *P. putida* data were fitted with the transport model (1–10), using the known parameter values $k_c = 0.78\,\text{h}^{-1}$, $\lambda = 0.0109\,\text{h}^{-1}$, and $\lambda^* = \lambda/2 = 0.0055\ \text{h}^{-1}$, and U as fitted from the tracer data to estimate the unknown parameters D_x, $D_y = D_z$, and k_r. The assumed relationships for the two decay rates were imposed by the need to reduce the number of unknown parameters to be fitted. All fitted and experimentally determined parameter values are listed in Table 2. The desired model aquifer dispersivities were determined to be: $\alpha_L = 4.54$ cm, and $\alpha_{Ty} = \alpha_{Tz} = 0.31$ cm. Fig. 12 shows the *P. putida* concentrations observed at sampling locations 14, 24, 26, and 56, in appropriate vertical $y - z$ planes at two different times together with the corresponding concentration contours predicted by the numerical transport model using the best-fitted parameter values. Similarly, Fig. 13 shows the *P. putida* concentrations observed at sampling locations 14, 26, 35, 43, 47, 56, and 82, in appropriate vertical $x - y$ planes at two different times. Figures 12 and 13 show relatively good agreement between the observed *P. putida* concentrations and the numerical solution.

The first and second normalized temporal moments were calculated from the experimental data collected at the various sampling locations shown in Fig. 9 for the tracer as well as for *P. putida*. The calculated ratios $M_{1(b)}/M_{1(t)}$, and $M_{2(b)}/M_{2(t)}$ are listed in Table 3. Clearly, the transport of *P. putida* is significantly retarded ($M_{1(b)}/M_{1(t)} > 1$) and spread more in the pilot-scale aquifer ($M_{2(b)}/M_{2(t)} > 1$) compared to chloride due to the attachment/detachment of *P. putida* onto quartz sand. Note that retarded breakthrough of bacteria compared to a conservative tracer has also been observed in other laboratory (Chen and Strevett 2002) and field-scale studies (Bales et al. 1995). This observed retardation can be attributed to attachment of bacteria onto the solid matrix (Harvey and Garabedian 1991; Silliman et al. 2001). For the experimental conditions of this study, straining cannot be considered an important

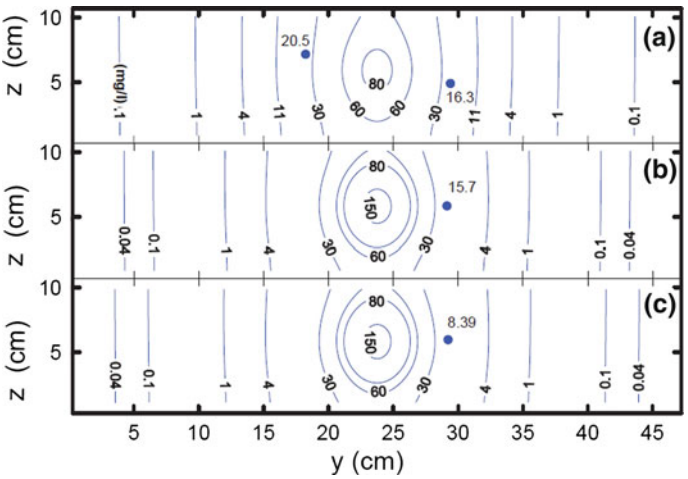

Fig. 10 Chloride concentration contour plots in mg/L, in various vertical $y-z$ planes of the bench scale aquifer and observed chloride concentrations at sampling locations indicated by the solid circles for **a** $t = 26$ h, $x = 23.9$ cm, showing SL 24 and SL 26, **b** $t = 26$ h, $x = 13.75$ cm, showing SL 14, and **c** $t = 48$ h, $x = 13.75$ cm, showing SL 14

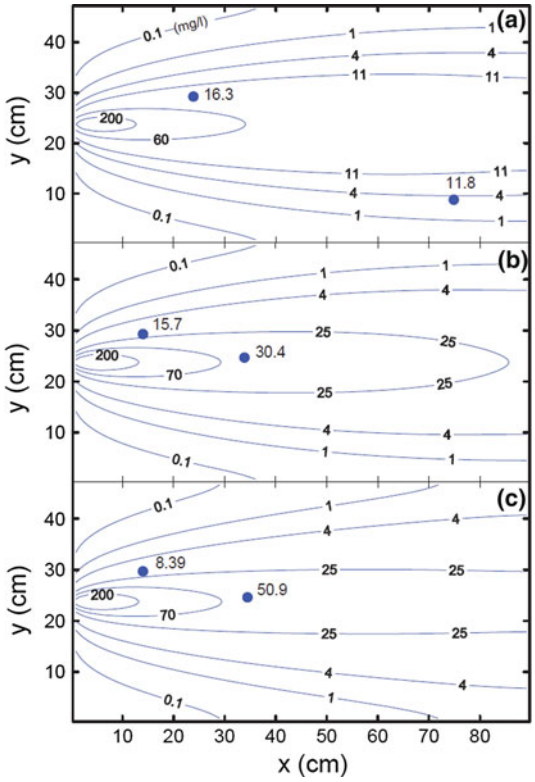

Fig. 11 Chloride concentration contour plots in mg/L, in various horizontal $x - y$ planes of the bench scale aquifer and observed chloride concentrations at sampling locations indicated by the *solid circles* for **a** $t = 26$ h, $z = 5$ cm, showing SL 24 and SL 78, **b** $t = 26$ h, $z = 6$ cm, showing SL 14 and SL 35, and **c** $t = 48$ h, $z = 6$ cm, showing SL 14 and SL 35

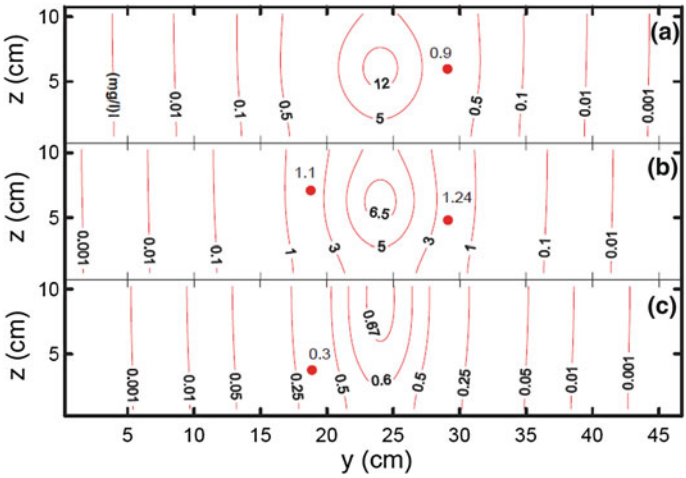

Fig. 12 *P. putida* concentration contour plots in mg/L, in various vertical $y-z$ planes of the bench scale aquifer and observed *P. putida* concentrations at sampling locations indicated by the *solid circles* for **a** $t = 48$ h, $x = 13.75$ cm, showing SL 14, **b** $t = 48$ h, $x = 23.9$ cm, showing SL 24 and SL 26, and **c** $t = 22$ h, $x = 54.35$ cm, showing SL 56

Fig. 13 *P. putida* concentration contour plots in mg/L, in various horizontal $x - y$ planes of the bench scale aquifer and observed *P. putida* concentrations at sampling locations indicated by the *solid circles* for **a** $t = 33.5$ h, $z = 4$ cm, showing SL 43 and 56, **b** $t = 48$ h, $z = 6$ cm, showing SL 14 and SL 35, and **c** $t = 48$ h, $z = 7$ cm, showing SL 26, SL 47, and SL 82

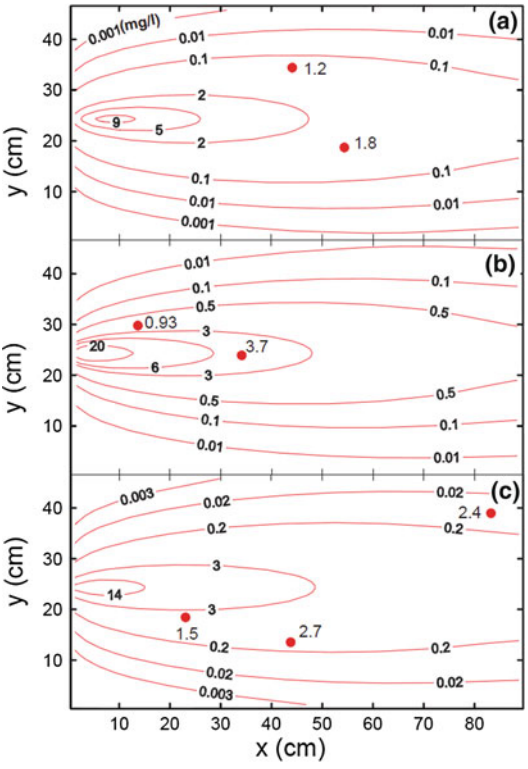

Table 3 Calculated moment ratios at the various sampling locations

Sampling location	$M_{1(b)}/M_{1(t)}$	$M_{2(b)}/M_{2(t)}$
SL14	1.8	3.1
SL24	1.9	3.7
SL35	1.7	3.0
SL43	1.7	2.9
SL56	1.5	2.5
SL65	1.5	2.3

mechanism of mass loss because the average size of the bacteria cells (2.16 μm) was approximately ~ 0.3 % of the median grain diameter of sand, d_c, which was considerably smaller than the 5 % limit recommended by Hendry et al. (1999) and Choi et al. (2007). In contrast, experimental observations suggest that straining may occur for much lower values of d_c/d_{50}. Li et al. (2004) observed straining for $d_c/d_{50} = 0.002$. Also, Tufenkji et al. (2004) reported that irregularity of the sand grain shape significantly contributes to the straining potential of porous media.

Worthy to note is that the tracer dispersivities ($\alpha_L = 8.46$ cm, $\alpha_{Ty} = \alpha_{Tz} = 0.45$ cm) were grater than those for *P. putida* ($\alpha_L = 4.54$ cm, and $\alpha_{Ty} = \alpha_{Tz} = 0.31$ cm), suggesting that the dispersivity is decreasing with particle size. This result is in perfect agreement with previous colloid and biocolloid transport studies published in the literature (Keller et al. 2004; Vasiliadou and Chrysikopoulos 2011; Syngouna and Chrysikopoulos 2011; Chrysikopoulos and Syngouna 2012).

7 Summary and Conclusions

The transport of *P. putida* bacterial cells in a 3-D, water saturated model aquifer, packed with quartz sand was investigated. The experimental data were adequately fitted with a 3-D finite-difference numerical model. The results of this study are of particular interest, as the transport of bacteria in water saturated bench scale 3-D model aquifer has not been extensively examined previously.

Pseudomonas putida cells are negatively charged due to cell wall constituents (phosphate and carboxyl groups, proteins). Because, quartz sand grains in aqueous media are also negatively charged, interactions between the surfaces of *P. putida* cells and sand grains should have been repulsive and thus unfavorable to adhesion. Therefore, if solely electrostatic interactions were involved, adhesion should not take place. Despite these predictions, our results showed that bacteria and quartz sand have a strong electron-donor character, and suggested the importance of Lewis acid–base interactions in adhesion of the *P. putida* to quartz sand. The XDLVO theory qualitatively predicted adhesion results better than the classical DLVO theory.

Acknowledgments This research has been co-financed by the European Union (European Social Fund-ESF) and Greek national funds through the Operational program "Education and Lifelong Learning" of the National Strategic Reference Framework (NSRF)-Research Funding Programs: Heracleitus II and Aristeia. Investing in knowledge society through the European Social Fund.

References

Anders, R., Chrysikopoulos, C.V.: Virus fate and transport during artificial recharge with recycled water. Water Resour. Res. **41**, W10415 (2005). doi:10.1029/2004WR003419

Anders, R., Chrysikopoulos, C.V.: Transport of viruses through saturated and unsaturated columns packed with sand. Transp. Porous Media **76**, 121–138 (2009)
Aronov, D., Rosen, R., Ron, E.Z., Rosenman, G.: Electron-induced surface modification of hydroxyapatite-coated implant. Surf. Coat. Technol. **202**, 2093–2102 (2008)
Auset, M., Keller, A.A.: Intermittent filtration of bacteria and colloids in porous media. Water Resour. Res. **41**, W09408 (2005). doi:10.1029/2004WR003611
Bales, R.C., Li, S., Maguire, K.M., Yahya, M.T., Gerba, C.P., Harvey, R.W.: Virus and bacteria transport in a sandy aquifer, Cape Cod, MA. Gr. Water **3**, 653–661 (1995)
Bear, J., Verruijt, A.: Modeling Groundwater Flow and Pollution. D. Reidel, Norwell, MA (1987)
Becker, M.W., Collins, S.A., Metge, D.W., Harvey, R.W., Shapiro, A.M.: Effect of cell physicochemical characteristics and motility on bacterial transport in groundwater. J. Contam. Hydrol. **69**, 195–213 (2004)
Bergendahl, J., Grasso, D.: Prediction of colloid detachment in a model porous media: thermodynamics. AIChE J. **45**, 475–484 (1999)
Bird, R.B., Stewart, W.E., Lightfoot, E.N.: Transport Phenomena, 2nd edn. Wiley, New York (2002)
Bolster, C.H., Haznedaroglu, B.Z., Walker, S.L.: Diversity in cell properties and transport behavior among 12 different environmental *Escherichia coli* isolates. J. Environ. Qual. **38**, 465–472 (2009)
Bradford, S., Simunek, J., Walker, S.L.: Transport and straining of *E. coli* O157:H7 in saturated porous media. Water Resour. Res. **42**, W12S11–12 (2006)
Bradford, S.A., Torkzaban, S., Walker, S.L.: Coupling of physical and chemical mechanisms of colloid straining in saturated porous media. Water Res. **41**, 3012–3024 (2007)
Brown, D.G., Abramson, A.: Collision efficiency distribution of a bacterial suspension flowing through porous media and implications for field-scale transport. Water Res. **40**, 1591–1598 (2006)
Bruggeman, D.A.G.: Berechnung verschiedener physikalischer Konstanten von heterogenen Substanzen. Ann. Phys. (Leipzig) **24**, 636–679 (1935)
Camesano, T., Logan, B.: Influence of fluid velocity and cell concentration on the transport of motile and nonmotile bacteria in porous media. Environ. Sci. Technol. **32**, 1699–1708 (1998)
Camesano, T., Unice, K.M., Logan, B.: Blocking and ripening of colloids in porous media and their implications for bacterial transport. Colloids Surf. A: Physicochem. Eng. Aspects **160**, 291–308 (1999)
Chen, G., Strevett, K.: Surface free energy relationships used to evaluate microbial transport. J Environ. Eng. **128**, 408–415 (2002)
Chen, G., Zhu, H.: Bacterial adhesion to silica sand as related to Gibbs energy variations. Colloids Surf. B: Biointerfaces **44**, 41–48 (2005)
Choi, N.H., Kim, D.J., Kim, S.B.: Quantification of bacterial mass recovery as a function of pore-water velocity and ionic strength. Res. Microbiol. **158**, 70–78 (2007)
Chrysikopoulos, C.V.: Artificial tracers for geothermal reservoir studies. Environ. Geol. **22**, 60–70 (1993)
Chrysikopoulos, C.V., Sim, Y.: One-dimensional virus transport homogeneous porous media with time dependent distribution coefficient. J. Hydrol. **185**, 199–219 (1996)
Chrysikopoulos, C.V., Syngouna, V.I.: Attachment of bacteriophages MS2 and ΦX174 onto kaolinite and montmorillonite: extended DLVO interactions. Colloids Surf. B: Biointerfaces **92**, 74–83 (2012)
Chrysikopoulos, C.V., Vogler, E.T.: Estimation of time dependent virus inactivation rates by geostatistical and resampling techniques: application to virus transport in porous media. Stoch. Environ. Res. Risk Assess. **18**(2), 67–78 (2004)
Chrysikopoulos, C.V., Lee, K.Y., Harmon, T.C.: Dissolution of a well-defined trichloroethylene pool in saturated porous media: experimental design and aquifer characterization. Water Resour. Res. **36**(7), 1687–1696 (2000)
Chrysikopoulos, C.V., Masciopinto, C., La Mantia, R., Manariotis, I.D.: Removal of biocolloids suspended in reclaimed wastewater by injection into a fractured aquifer model. Environ. Sci. Technol. **44**, 971–977 (2010)
Corapcioglu, M.Y., Kim, S.: Modeling facilitated contaminant transport by mobile bacteria. Water Resour. Res. **31**(11), 2639–2647 (1995)
Dela Barre, B.K., Harmon, T.C., Chrysikopoulos, C.V.: Measuring and modeling the dissolution of nonideally shaped dense nonaqueous phase liquid (NAPL) pools in saturated porous media. Water Resour. Res. **38**(8), 1133 (2002). doi:10.1029/2001WR000444
Derjaguin, B.V., Landau, L.D.: Theory of the stability of strongly charged lyophobic soils and of the adhesion of strongly charged particles in solutions of electrolytes. Acta Physicochim. U.S.S.R. **14**, 733–762 (1941)
Duba, A.G., Jackson, K.J., Jovanovich, M.C., Knapp, R.B., Taylor, R.T.: TCE remediation using in situ, resting-state bioaugmentation. Environ. Sci. Technol. **30**, 1982–1989 (1996)
Feke, D.L., Prabhu, N.D., Mann, J.A. Jr., Mann, J.A. III.: A formulation of the short-range repulsion between spherical colloidal particles. J. Phys. Chem. **88**, 5735–5739 (1984)

Fontes, D.E., Mills, A.L., Hornberger, G.M., Herman, J.S.: Physical and chemical factors influencing transport of microorganisms through porous media. Appl. Environ. Microbiol. **57**, 2473–2481 (1991)
Foppen, J.W.A., Schijven, J.F.: Transport of *E. coli* in columns of geochemically heterogeneous sediment. Water Res. **39**, 3082–3088 (2005)
Foppen, J.W.A., van Herwerden, M., Kebtie, M., Noman, A., Schijven, J.F., Stuyfzand, P.J., Uhlenbrook, S.: Transport of *Escherichia coli* and solutes during waste water infiltration in an urban alluvial aquifer. J. Contam. Hydrol. **95**, 1–16 (2008)
Gannon, J.T., Manilal, V.B., Alexander, M.: Relationships between cell surface properties and transport of bacteria through soil. Appl. Environ. Microbiol. **57**, 190–193 (1991)
Gargiulo, G., Bradford, S.A., Simunek, J., Ustohal, P., Vereecken, H., Klumpp, E.: Bacteria transport and deposition under unsaturated flow conditions: the role of water content and bacteria surface hydrophobicity. Vadose Zone J. **7**(2), 406–419 (2008)
Garrouch, A.A., Ali, L., Qasem, F.: Using diffusion and electrical measurements to assess tortuosity of porous media. Ind. Eng. Chem. Res. **40**, 4363–4369 (2001)
Ginn, T.R., Wood, B.D., Nelson, K.E., Scheibe, T.D., Murphy, E.M., Glement, T.P.: Processes in microbial transport in the natural subsurface. Adv. Water Resour. **25**, 1017–1042 (2002)
Gregory, J.: Approximate expressions for retarded van der Waals interaction. J. Colloid Interf. Sci. **83**, 138–145 (1981)
Harvey, R.W., Garabedian, S.P.: Use of colloid filtration theory in modeling movement of bacteria through a contaminated sandy aquifer. Environ. Sci. Technol. **25**, 178–185 (1991)
Harvey, R.W., Kinner, N.E., MacDonald, D., Metge, D.W., Bunn, A.: Role of physical heterogeneity in the interpretation of small-scale laboratory and field observations on bacteria, microbial-sized microsphere, and bromide transport through aquifer sediments. Water Resour. Res. **29**, 2713–2721 (1993)
Harvey, R.W., Metge, D.W., Barber, L.B., Aiken, G.R.: Effects of altered groundwater chemistry upon the pH-dependency and magnitude of bacterial attachment during transport within an organically contaminated sandy aquifer. Water Res. **44**, 1062–1071 (2010)
Haas, C.N.: Moment analysis of tracer experiments. J. Environ. Eng. ASCE **122**, 1121–1123 (1996)
Haznedaroglu, B.Z., Kim, H.N., Bradford, S.A., Walker, S.L.: Relative transport behavior of *Escherichia coli* O157:H7 and *Salmonella enterica Serovar Pullorum* in packed bed column systems: influence of solution chemistry and cell concentration. Environ. Sci. Technol. **43**, 1838–1844 (2009)
Hendry, M.J., Lawrence, J.R., Maloszewski, P.: Effect of velocity on the transport of two bacteria through saturated sand. Gr. Water. **37**, 103–112 (1999)
Hogg, R., Healy, T.W., Fuerstenau, D.W.: Mutual coagulation of colloidal dispersions. Trans. Faraday Soc. **62**, 1638–1651 (1966)
Hubbard, S.S., Chen, J., Peterson, J., Majer, E.L., Williams, K.H., Swift, D.J., Mailloux, B., Rubin, Y.: Hydrogeological characterization of the South Oyster bacterial transport site using geophysical data. Water Resour. Res. **37**, 2431–2456 (2001)
Huyakorn, P.S., Pinder, G.F.: Computational Methods in Subsurface Flow. Academic Press, San Diego (1983)
Israelachvili, J.N.: Intermolecular and Surface Forces, 2nd edn. Academic Press, London (1992)
James, S.C., Chrysikopoulos, C.V.: Monodisperse and polydisperse colloid transport in water-saturated fractures with various orientations: gravity effects. Adv. Water Resour. **34**, 1249–1255 (2011). doi:10.1016/j.advwatres.2011.06.001
Jewett, D.G., Hilbert, T.A., Logan, B.E., Arnold, R.G., Bales, R.C.: Bacterial transport in laboratory columns and filters: Influence of ionic strength and pH on collision efficiency. Water Res. **29**, 1673–1680 (1995)
Johnson, W.P., Zhang, P., Fuller, M.E., Scheibe, T.D., Mailloux, B.J., Onstott, T.C., DeFlaun, M.F., Hubbard, S.S., Radtke, J., Kovacik, W.P., Holben, W.: Ferrographic tracking of bacterial transport in the field at the narrow channel focus area, Oyster, VA. Environ. Sci. Technol. **35**, 182–191 (2001)
Jucker, B.A., Zehnder, A.J.B., Harms, H.: Quantification of polymer interactions in bacterial adhesion. Environ. Sci. Technol. **32**, 2909–2915 (1998)
Keller, A.A., Sirivithayapakorn, S., Chrysikopoulos, C.V.: Early breakthrough of colloids and bacteriophage MS2 in a water saturated sand column. Water Resour. Res. **40**, W08304 (2004). doi:1029/2003WR002676
Kim, H.N., Bradford, S.A., Walker, S.L.: *Escherichia coli* 0157:h7 transport in saturated porous media: role of solution chemistry and surface macromolecules. Environ. Sci. Technol. **43**, 4340–4347 (2009)
Kim, H.N., Walker, S.L., Bradford, S.A.: Macromolecule mediated transport and retention of *Escherichia coli* O157:H7 in saturated porous media. Water Res. **44**, 1082–1093 (2010)
Kim, S.B., Park, S.J., Lee, C.G., Choi, N.C., Kim, D.J.: Bacteria transport through goethite-coated sand: effects of solution pH and coated sand content. Colloids Surf. B: Biointerfaces **63**, 236–242 (2008)
Kuznar, Z.A., Elimelech, M.: Direct microscopic observation of particle deposition in porous media: role of the secondary energy minimum. Colloid Surf. A: Physicochem. Eng. Asp. **294**, 156–162 (2007)

Lee, K.Y., Chrysikopoulos, C.V.: Dissolution of a well-defined trichloroethylene pool in saturated porous media: experimental results and model simulations. Water Res. **36**, 3911–3918 (2002)
Lee, K.Y., Chrysikopoulos, C.V.: Dissolution of a multicomponent DNAPL pool in an experimental aquifer. J. Hazard. Mater. **B128**, 218–226 (2006)
Li, Q., Logan, B.E.: Enhancing bacterial transport for bioaugmentation of aquifers using low ionic strength solutions and surfactants. Water Res. **33**, 1090–1100 (1999)
Li, X., Scheibe, T.D., Johnson, W.P.: Apparent decreases in colloid deposition rate coefficients with distance of transport under unfavorable deposition conditions: a general phenomenon. Environ. Sci. Technol. **38**, 5616–5625 (2004)
Liu, Y., Yang, C.H., Li, J.: Influence of extracellular polymeric substances on *Pseudomonas aeruginosa* transport and deposition profiles in porous media. Environ. Sci. Technol. **41**, 198–205 (2007)
Loveland, J.P., Ryan, J.N., Amy, G.L., Harvey, R.W.: The reversibility of virus attachment to mineral surfaces. Colloids Surf. A: Physicochem. Eng. Asp. **107**, 205–221 (1996)
Masciopinto, C., La Mantia, R., Chrysikopoulos, C.V.: Fate and transport of pathogens in a fractured aquifer in the Salento area, Italy. Water Resour. Res. **44**, W01404 (2008). doi:10.1029/2006WR005643
Maxwell, R., Welty, C., Harvey, R.: Revisiting the Cape Cod bacteria injection experiment using a stochastic modeling approach. Environ. Sci. Technol. **41**(15), 5548–5558 (2007)
Mailloux, B.J., Fuller, M.E., Onstott, T.C., Hall, J., Dong, H., DeFlaun, M.F., Streger, S.H., Rothmel, R.K., Green, M., Swift, D.J.P., Radke, J.: The role of physical, chemical, and microbial heterogeneity on the field-scale transport and attachment of bacteria. Water Resour. Res. **39**(6), 1142 (2003). doi:10.1029/2002WR001591
Mills, A.L, Herman, J.S, Horneberger, G.M, Dejesust, T.H.: Effect of solution ionic strength and iron coatings on mineral grains on the sorption of bacterial cells to quartz sand. Appl. Environ. Microbiol. **60**, 3300–3306 (1994)
Pavelic, P., Dilon, P.J., Barry, K.E., Vanderzalm, J.L., Correll, R.L., Rinck-Pfeiffer, M.: Water quality effects on clogging rates during reclaimed water ASR in a carbonate aquifer. J. Hydrol. **334**, 1–16 (2007)
PEST: Model-independent parameter estimation user manual, 5th edn. Watermark Numerical Computing, Brisbane (2010)
Pisani, L.: Simple expression for the tortuosity of porous media. Transp. Porous Med. **88**, 193–203 (2011)
Powelson, D.K., Mills, A.L.: Transport of *Escherichia coli* in sand columns with constant and changing water contents. J. Environ. Qual. **30**, 238–245 (2001)
Rogers, B., Logan, B.E.: Bacterial transport in NAPL-contaminated porous media. J. Environ. Eng. **126**, 657–666 (2000)
Redman, J.A., Grant, S.B., Olson, T.M., Estes, M.K.: Pathogen filtration, heterogeneity, and the potable reuse of wastewater. Environ. Sci. Technol. **35**, 1798–1805 (2001)
Redman, J.A., Walker, S.L., Elimelech, M.: Bacterial adhesion and transport in porous media: role of the secondary energy minimum. Environ. Sci. Technol. **38**, 1777–1785 (2004)
Rong, X., Huanga, Q., He, X., Chen, H., Cai, P., Liang, W.: Interaction of *Pseudomonas putida* with kaolinite and montmorillonite: a combination study by equilibrium adsorption, ITC, SEM and FTIR. Colloids Surf. B: Biointerfaces **64**, 49–55 (2008)
Ruckenstein, E., Prieve, D.C.: Adsorption and desorption of particles and their chromatographic separation. AIChE J. **22**, 276–283 (1976)
Russel, W.B., Saville, D.A., Schowalter, W.R.: Colloidal Dispersions. Cambridge University Press, Cambridge (1989)
Ryan, J.N., Gschwend, P.M.: Effects of ionic strength and flow rate on colloid release: relating kinetics to intersurface potential energy. J. Colloid Interf. Sci. **164**, 21–34 (1994)
Schinner, T., Letzner, A., Liedtke, S., Castro, F.D., Eydelnant, I.A., Tufenkji, N.: Transport of selected bacterial pathogens in agricultural soil and quartz sand. Water Res. **44**, 1182–1192 (2010)
Silliman, S.E., Dunlap, R., Fletcher, M., Schneegurt, M.A.: Bacterial transport in heterogeneous porous media: observations from laboratory experiments. Water Resour. Res. **37**, 2699–2707 (2001)
Sim, Y., Chrysikopoulos, C.V.: Analytical models for one-dimensional virus transport in saturated porous media. Water. Resour. Res. **31**, 1429–1437 (1995). (Correction, Water Resour. Res. **32**, 1473 (1996))
Sim, Y., Chrysikopoulos, C.V.: Three-dimensional analytical models for virus transport in saturated porous media. Transp. Porous Med. **30**, 87–112 (1998)
Sim, Y., Chrysikopoulos, C.V.: Analytical solutions for solute transport in saturated porous media with semi-infinite or finite thickness. Adv. Water Resour. **22**, 507–519 (1999)
Sim, Y., Chrysikopoulos, C.V.: Virus transport in unsaturated porous media. Water Resour. Res. **36**(1), 173–179 (2000)
Simoni, S.F., Harms, H., Bosma, T.N.P., Zehnder, A.J.B.: Population heterogeneity affects transport of bacteria through sand columns at low flow rates. Environ. Sci. Technol. **32**, 2100–2105 (1998)

Stephan, E.A., Chase, G.G.: A preliminary examination of zeta potential and deep bed filtration activity. Separation Purification Technol. **21**, 219–226 (2001)
Stevik, T.K., Aa, K., Ausland, G., Hanssen, J.F.: Retention and removal of pathogenic bacteria in wastewater percolating through porous media: A review. Water Res. **38**, 1355–1367 (2004)
Stumpp, C., Lawrence, J.R., Hendry, M.J., Maloszewski, P.: Transport and bacterial interactions of three bacterial strains in saturated column experiments. Environ. Sci. Technol. **45**, 2116–2123 (2011)
Swanton, S. W.: Modeling colloid transport in groundwater: the prediction of colloid stability and retention behavior. Adv. Colloid Interf. Sci. **54**, 129–208 (1995)
Syngouna, V.I., Chrysikopoulos, C.V.: Interaction between viruses and clays in static and dynamic batch systems. Environ. Sci. Technol. **44**, 4539–4544 (2010)
Syngouna, V.I., Chrysikopoulos, C.V.: Transport of biocolloids in water saturated columns packed with sand: effect of grain size and pore water velocity. J. Contamin. Hydrol. **126**, 301–314 (2011)
Tong, M., Li, X., Brow, C.N., Johnson, W.P.: Detachment-influenced transport of an adhesion-deficient bacterial strain within water-reactive porous media. Environ. Sci. Technol. **39**, 2500–2508 (2005)
Torkzaban, S., Tazehkand, S.S., Walker, S.L., Bradford, S.A.: Transport and fate of bacteria in porous media: coupled effects of chemical conditions and pore space geometry. Water Resour. Res. **44**, W04403 (2008). doi:04410.01029/02007WR006541
Torkzaban, S., Kim, H.N., Simunec, J., Bradford, S.A.: Hysteresis of colloid retention and release in saturated porous media during transients in solution chemistry. Environ. Sci. Technol. **44**, 1662–1669 (2010)
Tufenkji, N.: Modeling microbial transport in porous media: traditional approaches and recent developments. Adv. Water Resour. **30**, 1455–1469 (2007)
Tufenkji, N., Miller, G.F., Ryan, J.N., Harvey, R.W., Elimelech, M.: Transport of Cryptosporidium oocysts in porous media: role of straining and physicochemical filtration. Environ. Sci. Technol. **38**, 5932–5938 (2004)
van der Mei, H.C., Bos, R., Busscher, H.J.: A reference guide to microbial cell surface hydrophobicity based on contact angles. Colloids Surf. B: Biointerfaces **11**, 213–221 (1998)
van Oss, C.J.: Energetics of cell-cell and cell-biopolymer interactions. Cell Biophys. **14**(1), 1–16 (1989)
van Oss, C.J.: Acid-base interracial interactions in aqueous media. Colloids Surf. A: Physicochem. Eng. Asp. **78**, 1–49 (1993)
van Oss, C.J.: Interfacial Forces in Aqueous Media. Marcel Dekker, New York (1994)
van Oss, C.J., Giese, R.F.: Role of the properties and structure of liquid water in colloidal and interracial systems. J. Dispersion Sci. Technol. **25**(5), 631–655 (2004)
van Oss, C.J., Giese, R.F., Costanzo, P.M.: DLVO and non-DLVO interactions in hectorite. Clays Clay Miner. **38**, 151–159 (1990)
Vasiliadou, I.A., Chrysikopoulos, C.V.: Cotransport of *Pseudomonas putida* and kaolinite particles through water saturated columns packed with glass beads. Water Resour. Res. **47**, W02543 (2011). doi:10.1029/2010WR009560
Vasiliadou, I.A., Papoulis, D., Chrysikopoulos, C.V., Panagiotaras, D., Karakosta, E., Fardis, M., Papavassiliou, G.: Attachment of *Pseudomonas putida* onto differently structured kaolinite minerals: a combined ATR-FTIR and ^{1}H NMR study. Colloids Surf. B: Biointerfaces **84**(2), 354–359 (2011). doi:10.1016/j.colsurfb.2011.01.026
Verwey, E.J., Overbeek, J.T.G.: Theory of the stability of lyophobic colloids. Elsevier, Amsterdam (1948)
Wilke, C.R., Chang, P.: Correlation of diffusion coefficients in dilute solutions. AIChE J. **1**, 264–270 (1955)
Yoon, R.-H., Flin, D.H., Rabinovich, Y.I.: Hydrophobic interactions between dissimilar surfaces. J. Colloid Interf. Sci. **185**, 363–370 (1997)
Zhang, P., Johnson, W.P., Scheibe, T.D., Choi, K.-H., Dobbs, F.C., Mailloux, B.J.: Extended tailing of bacteria following breakthrough at the narrow channel focus area, Oyster, Virginia. Water Resour. Res. **37**(11), 2687–2698 (2001)
Zheng, C., Bennet, G.D.: Applied contaminant transport modeling. Van Nostrand Reinhold ITP, New York (1995)